

# Nanoporous Block Copolymer Membranes with Enhanced Solvent Resistance Via UV-Mediated Cross-Linking Strategies

Florian V. Frieß, Qiwei Hu, Jannik Mayer, Lea Gemmer, Volker Presser, Bizan N. Balzer,\* and Markus Gallei\*

In this work, a block copolymer (BCP) consisting of poly((butyl methacrylate-*co*-benzophenone methacrylate-*co*-methyl methacrylate)-*block*-(2-hydroxyethyl methacrylate)) (P(BMA-*co*-BPMA-*co*-MMA)-*b*-P(HEMA)) is prepared by a two-step atom-transfer radical polymerization (ATRP) procedure. BCP membranes are fabricated applying the self-assembly and nonsolvent induced phase separation (SNIPS) process from a ternary solvent mixture of tetrahydrofuran (THF), 1,4-dioxane, and dimethylformamide (DMF). The presence of a porous top layer of the integral asymmetric membrane featuring pores of about 30 nm is confirmed via scanning electron microscopy (SEM). UV-mediated cross-linking protocols for the nanoporous membrane are adjusted to maintain the open and isoporous top layer. The swelling capability of the noncross-linked and cross-linked BCP membranes is investigated in water, water/ethanol mixture (1:1), and pure ethanol using atomic force microscopy, proving a stabilizing effect of the UV cross-linking on the porous structures. Finally, the influence of the herein described cross-linking protocols on water-flux measurements for the obtained membranes is explored. As a result, an increased swelling resistance for all tested solvents is found, leading to an increased water flux compared to the pristine membrane. The herein established UV-mediated cross-linking protocol is expected to pave the way to a new generation of porous and stabilized membranes within the fields of separation technologies.

## 1. Introduction

Currently, polymer membranes attracted enormous attention for separating components from water or organic solvents.<sup>[1]</sup> Porous and sponge-like polymer membranes can be prepared by the so-called nonsolvent induced phase separation (NIPS) or thermally induced phase separation (TIPS) processes for industrially relevant applications. Ultrafiltration membranes typically feature pore sizes in the range of 5–100 nm, and they have attracted attention for the removal of colloids, organic contaminants, and macromolecules in the field of wastewater treatment and remediation, or selective separations.<sup>[2–4]</sup> Block copolymers (BCPs) represent an exciting class of polymers to prepare iso- and nanoporous films with well-defined and adjustable pore sizes. Moreover, these pores may be reversibly changed regarding the polarity and size through incorporation of smart and functional polymer segments.<sup>[5–9]</sup> Asymmetric copolymer membranes can be obtained by application of the combination of BCP self-assembly and nonsolvent induced phase separation (SNIPS) process.<sup>[10]</sup> For this


F. V. Frieß, L. Gemmer, M. Gallei  
Department of Chemistry  
Saarland University  
66123 Saarbrücken, Germany  
E-mail: markus.gallei@uni-saarland.de

F. V. Frieß, L. Gemmer, V. Presser, M. Gallei  
Saarene  
Saarland Center for Energy Materials and Sustainability  
Campus C4 2, 66123 Saarbrücken, Germany

Q. Hu, B. N. Balzer  
Institute of Physical Chemistry  
University of Freiburg  
Albertstraße 21, 79104 Freiburg, Germany  
E-mail: bizan.balzer@physchem.uni-freiburg.de

Q. Hu, B. N. Balzer  
Cluster of Excellence livMatS @ FIT-Freiburg Center for Interactive  
Materials and Bioinspired Technologies  
University of Freiburg  
Georges-Köhler-Allee 105, 79110 Freiburg, Germany

J. Mayer  
Ernst-Berl-Institute of Chemical Engineering and Macromolecular  
Chemistry  
Technische Universität Darmstadt  
Alarich-Weiss-Straße 4, 64287 Darmstadt, Germany  
V. Presser  
Department of Materials Science and Engineering  
Saarland University  
Campus D2 2, 66123 Saarbrücken, Germany

 The ORCID identification number(s) for the author(s) of this article can be found under <https://doi.org/10.1002/marc.202100632>

© 2021 The Authors. Macromolecular Rapid Communications published by Wiley-VCH GmbH. This is an open access article under the terms of the Creative Commons Attribution License, which permits use, distribution and reproduction in any medium, provided the original work is properly cited.

DOI: 10.1002/marc.202100632

purpose, a concentrated polymer solution is cast on a macroporous support followed by immersion in a nonsolvent bath. This procedure is accompanied by a microphase separation of the BCP, forming a selective layer with uniform pores at the top of the substrate.<sup>[5,7,11]</sup> For more details on the membrane formation process and potential applications, readers are referred to some excellent reviews and articles in this field.<sup>[12–17]</sup> A major issue for these membranes is the structural change upon applying high pressure, temperatures above the glass transition temperature,  $T_g$ , and the missing long-term stability.<sup>[18]</sup> To a certain extent, this can be circumvented by increasing the  $T_g$  of the matrix-forming block segment, which in principle determines the mechanical properties of the thin porous layer. Abetz and co-workers, for instance, explored the feasibility of BCPs based on poly( $\alpha$ -methylstyrene)- and poly(4-methylstyrene) with poly(4-vinylpyridine) as polar block segment to increase the thermal membrane stability up to 150 °C.<sup>[19]</sup> In another study, Zhou et al. reported increasing thermal membrane stability up to 158 °C by using poly(styrene-*alt*-*N*-phenylmaleimide) as a matrix-forming block segment.<sup>[20]</sup> A different approach is represented by UV-induced cross-linking strategies for stabilizing BCP architectures, such as micelles or capsules. For example an anthracene motif was used by Elter et al. in a methoxy-poly(ethylene oxide)-*block*-poly(2-ethylhexyl glycidyl ether-*co*-9-methylanthracenyl glycidyl ether) diblock terpolymer to form partially reversible cross-links in the micelle cores.<sup>[21]</sup> Chen et al. used poly(styrene-*co*-benzophenone) as the hydrophobic block to prepare stabilized micelles through photo-cross-linking to increase (water) concentration and heat stability, and long-term storage.<sup>[22]</sup> Kang et al. were able to synthesize core cross-linked micelles from poly(ethylene oxide)-*block*-poly(2-[4'-iodobenzoyloxy]-ethyl methacrylate) generating benzophenone moieties, which were exploited to immobilize the polymer on silicon wafers.<sup>[23]</sup> By incorporating a polymerizable allyl group between the two block segments of stimuli-responsive poly(vinyl ferrocene)-*block*-poly(ethylene glycol), Morsbach et al. significantly stabilized the BCP micelle by using UV cross-linking protocols.<sup>[24]</sup> Yang et al. showed an increased pressure resistance (up to 2 bar) of membranes against various organic solvents, such as dimethylformamide (DMF) and toluene, as well as resistance to acetic acid and dilute base via preparation and annealing of a poly(*S*-*block*-poly(methyl methacrylate)). During this process, the polystyrene (PS) block formed cross-linking sites.<sup>[25]</sup> However, to the best of our knowledge, benzophenone as an integral part of the nonpolar (co)polymer segment was not reported for isoporous BCP membranes.

In this work, we present a synthetic procedure for an intrinsically UV cross-linkable amphiphilic BCP and applied the SNIPS process to combine the advantages of the convenient preparation of BCP membranes and increased stability of the cross-linkable matrix-forming polymer segment. For the hydrophobic block, a statistical copolymer, consisting of methyl methacrylate (MMA), *n*-butyl methacrylate (BMA), and benzophenone methacrylate (BPMA) was chosen, while for the hydrophilic

block, 2-hydroxyethyl methacrylate (HEMA) was selected. Incorporating poly(HEMA) as the pore-forming cylindrical domain in BCP membranes was shown to offer advantages in subsequent post functionalization chemistry, antifouling properties, and access to filtration processes with a high water flux.<sup>[8,26–28]</sup>

## 2. Results and Discussion

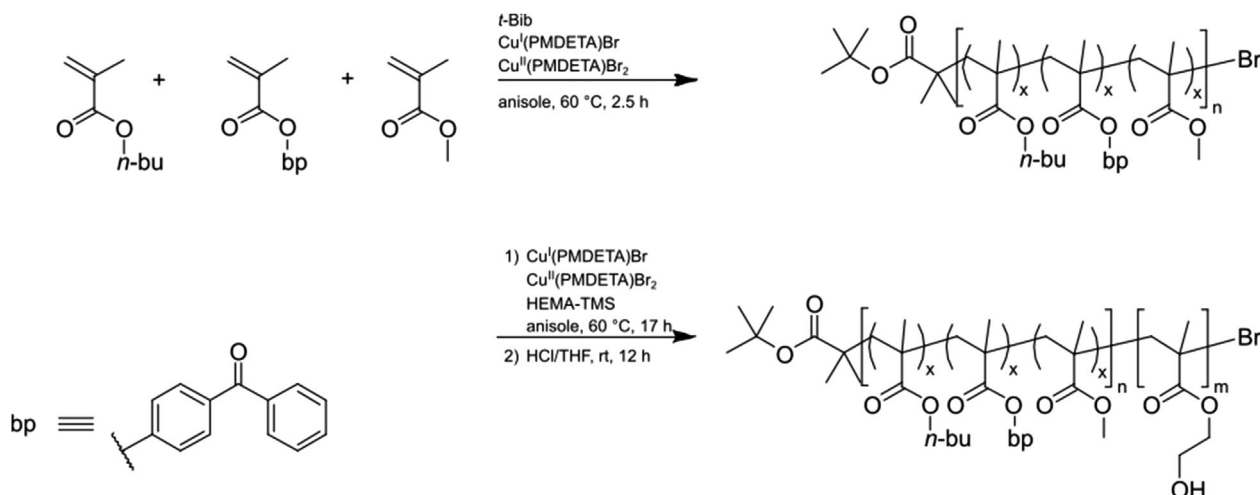
The amphiphilic BCP poly((butyl methacrylate-*co*-benzophenone methacrylate-*co*-methyl methacrylate)-*block*-(2-hydroxyethyl methacrylate)) P(BMA-*co*-BPMA-*co*-MMA)-*b*-P(HEMA) **P2** was synthesized via a two-step atom-transfer radical polymerization (ATRP), as shown in **Scheme 1**.

First, the statistical copolymer **P1** consisting of methyl *n*-butyl methacrylate (BMA) **1**, benzophenone methacrylate (BPMA) **2**, and methacrylate (MMA) **3** was polymerized by using *tert*-butyl  $\alpha$ -bromoisobutyrate (*t*Bib) as initiator, a mixture of Cu(I) and Cu(II)-bromide with *N,N,N',N',N''*-pentamethyldiethylenetriamine (PMDETA) ligands as catalyst and anisole as solvent. The incorporation of MMA and BMA as part of the macroinitiator offers two advantages: i) combining a high  $T_g$  and low  $T_g$  component (PMMA and PBMA respectively) increases the fracture resistance of polymer membranes for a poly(isoprene-*b*-styrene-*b*-4-vinylpyridine) terpolymer.<sup>[29]</sup> ii) The increased number of protons of BMA inside the polymer side-chain prevents main-chain scission during the cross-linking process, as shown by Carbone et al. when comparing PS- and poly(*n*-butyl acrylate)-based polymers for benzophenone-mediated UV cross-linking strategies.<sup>[30]</sup> Additionally, the benzophenone moieties are known for their efficient cross-linking capabilities upon UV-irradiation, without the necessity of the addition of radical starters or catalysts.<sup>[22,23,31–33]</sup> Within this study, the benzophenone moiety was additionally incorporated as an UV cross-linkable monomer to avoid leaching during application of the SNIPS process and to avoid any potential gradients of the small molecule within the final membrane structure. Moreover, the BPMA was only incorporated into the matrix-forming block segment of the membrane so that the pore-forming polar block segment was unaffected.

After purification and analysis of the statistical cross-linkable polymer **P1**, a second ATRP was carried out with (trimethylsiloxy ethyl) methacrylate (HEMA-TMS) as monomer, using a similar catalyst system (see Scheme 1 and Supporting Information for further details). After BCP formation, the P(HEMA-TMS) block was deprotected with hydrochloric acid, yielding the targeted amphiphilic block copolymer **P2**. The obtained polymer was analyzed concerning its chemical composition via <sup>1</sup>H-NMR-spectroscopy and molecular weight and distribution via size exclusion chromatography (SEC). Corresponding analytical data are compiled in **Figure 1**.

The narrow molecular weight distribution of **P1** ( $\mathcal{D} = 1.23$ ) indicated a good control over the ATRP reaction. The SEC traces of **P2**, shown in Figure 1a), exhibited a clear shift to higher molar masses. The hydroxy-groups of the poly(HEMA) block, present in **P2** and to a small extent in the TMS-protected **P2**, interfered with the SEC analysis leading to nonrepresentative absolute molecular weights. Therefore, the hydroxyl groups of HEMA were protected with a stable benzoyl group (**P2-benz**), as described by Schöttner et al. for other HEMA-containing BCPs.<sup>[27]</sup> The weak

V. Presser  
INM – Leibniz-Institute for New Materials  
Campus D2 2, 66123 Saarbrücken, Germany



**Scheme 1.** Synthetic route leading to P(BMA-co-BPMA-co-MMA)-b-P(HEMA) via a two-step ATRP method. In the first step, a macroinitiator from methyl methacrylate (MMA), butyl methacrylate (BMA), and benzophenone methacrylate (BPMA) is synthesized and used in the second step to initiate polymerization of (trimethylsiloxy ethyl) methacrylate (HEMA-TMS).

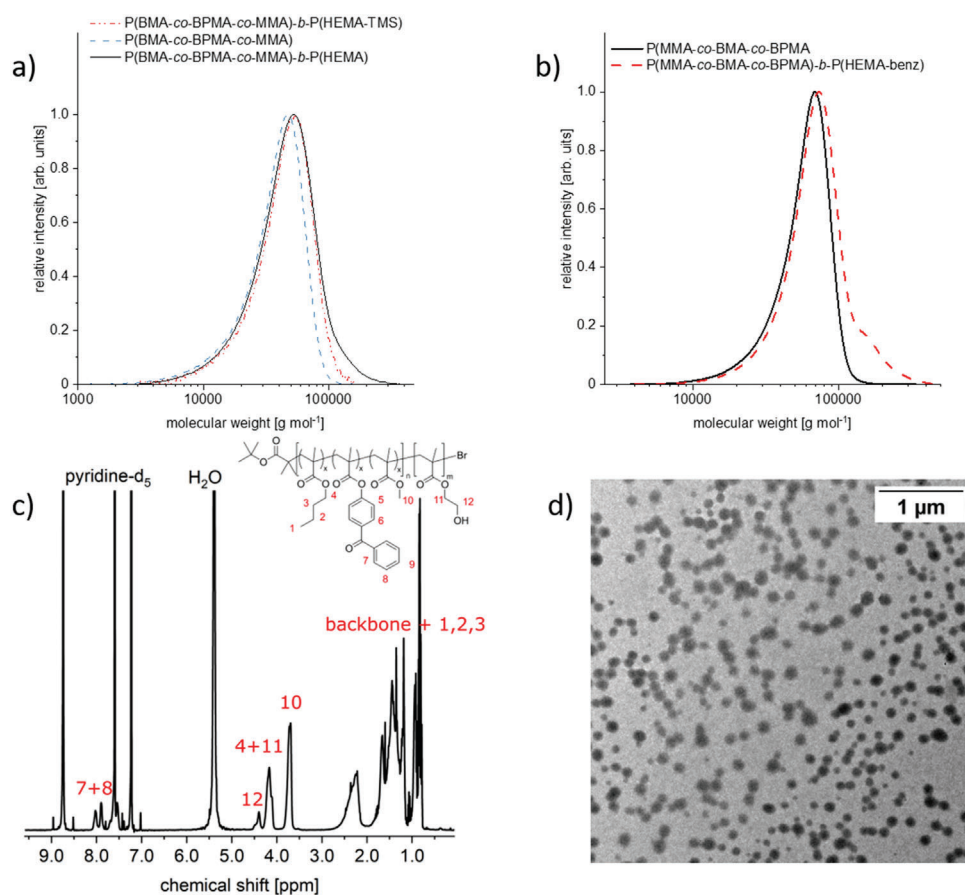


**Figure 1.** Analytical data. a) Molecular weight distribution of the macroinitiator P1 (blue, dashed), the BCP P2 (black, solid), and the TMS-protected BCP (red, dotted), obtained by SEC in DMF versus PMMA b) molecular weight distribution of the macroinitiator P1 (black, solid) and the benzoyl protected BCP P2-benz (red, dashed), obtained by SEC versus PS in THF c)  $^1\text{H}$ -NMR spectrum of P2 measured in pyridine- $d_5$  at 300 MHz and 300 K. d) Transmission electron micrograph of P2 micelles obtained from a ternary solvent mixture of THF, DMF and 1,4-dioxane (2:1:1 by mass).

**Table 1.** Summary of the relevant data for the block copolymer **P2**. For the calculation methods, please see the Supporting Information. Amounts for BMA, BPMA, and MMA repeating units corresponded to polymer **P1**. The amount of substance of the poly(HEMA) block in polymer **P2** was comparable to **P1**.

| $M_n(\text{P1})$<br>[g mol <sup>-1</sup> ] | $\bar{D}(\text{P1})$ | $M_n(\text{P2})$<br>[g mol <sup>-1</sup> ] | $\bar{D}(\text{P2-benz})$ | $M_n(\text{P2})_{\text{calc.}}$<br>[g mol <sup>-1</sup> ] |
|--|----------------------|--|---------------------------|---|
| 49 800                                     | 1.23                 | 59 400                                     | 1.33                      | 55 100  |
| x(BMA)                                     | x(BPMA)              | x(MMA)                                     | x(HEMA)                   | $\Phi(\text{HEMA})$                                       |
| 0.41                                       | 0.10                 | 0.49                                       | 0.10                      | 0.08  |

signal shifting toward higher  $M_n$  in the distribution of **P2-benz** could most likely be attributed to cross-linking reactions over the hydroxyl-groups during the protection procedure, as they were not observed within the molar mass distributions of the unprocessed and deprotected **P2**, shown in Figure 1a). The number average molecular weight of the benzoyl-protected polymer was determined to be 59 400 g mol<sup>-1</sup> with a polydispersity of 1.33, as determined by SEC in tetrahydrofuran (THF) versus PS. The molar fractions of the four polymer components were calculated after performing <sup>1</sup>H-NMR spectroscopy. It could be calculated from the corresponding integrals (Figure S1, Supporting Information) that the amount of the UV-cross-linking agent BPMA was about 10 mol% within the macroinitiator **P1**, together with 49 mol% MMA and 41 mol% BMA, whereas the hydrophilic block consisting of poly(HEMA) was determined to be 10 mol% for the overall BCP **P2**. The 10 mol% content of the BPMA was used based on previously reported studies revealing good mechanical properties for the investigated films. Within these studies contents between 0.5 and 20 mol% were investigated.<sup>[34,35]</sup>

A detailed calculation can be found, together with differential scanning calorimetry data (Figure S2, Supporting Information), in the Supporting Information. Traditionally, the hydrophilic block is incorporated with higher amounts. Yet, Plank et al. showed that poly(HEMA) forms cylindrical morphologies at significantly lower contents compared to typical phase diagrams of diblock copolymers.<sup>[36]</sup> The molar mass of the deprotected second poly(HEMA) block was calculated to be 5300 g mol<sup>-1</sup> using the SEC data and the <sup>1</sup>H-NMR spectral data (calculations can be found in the Supporting Information). In summary to the polymer synthesis and analytics, the obtained values for the composition were in good accordance with expectations based on the respective monomers used.

The volume fraction of the poly(HEMA) block segment of **P2** was calculated using the densities of the two respective blocks. While the density of **P1** was determined as 1.09 g cm<sup>-3</sup> following a method by Hughes,<sup>[37]</sup> literature data were used for the pure poly(HEMA) segment.<sup>[38]</sup> All data on the polymers are compiled in Table 1.

Before applying the SNIPS process for membrane formation, the micellation of **P2** was investigated in a ternary solvent mixture consisting of THF, DMF, and 1,4-dioxane in a 2:1:1 mass ratio, following a procedure by Schöttner et al. for another poly(HEMA)-containing block copolymer.<sup>[24]</sup> This solvent composition also represents the casting solution within the subsequent section. For transmission electron microscopy (TEM) stud-

ies, the polymer solution (30 wt-% of **P2** in the ternary mixture of solvents) was diluted by dropwise addition of the polymer solution into neat solvent mixture until a mass concentration of 2 mg L<sup>-1</sup> was reached. This solution was drop-casted on a carbon-coated copper grid, and the solvent was allowed to evaporate at ambient conditions for 12 h. Figure 1d displays a representative transmission electron micrograph of the resulting spherical micelles featuring a diameter of 127 ± 22 nm. In conclusion to the TEM investigations, micelle formation capabilities were proven for the amphiphilic BCPs, a basic prerequisite for BCP membrane formation using the SNIPS process.<sup>[16]</sup>

In the next step, BCP membranes from **P2** were fabricated. For this purpose, a 30 wt-% polymer solution of the ternary solvent mixture was prepared. The solution contained 0.43 wt-% CuCl<sub>2</sub> to increase the polymer solution's viscosity and enhance the order of the pores.<sup>[27,39]</sup> The viscous solution was cast on a polyester non-woven or cellulose support utilizing a doctor blade with 200 μm gap width. After a solvent evaporation time of 10 or 15 s, the polymer membrane was precipitated in deionized water for 30 min, predried at ambient conditions for 12 h, and then dried in a vacuum oven at 40 °C for 2 days.

The porous structure of the obtained membranes was investigated by scanning electron microscopy (SEM), shown in Figure 2.

As can be concluded from the corresponding SEM images Figure 2a,b, the topographies of the membranes exhibited an open-porous surface structure with pore sizes of 26 ± 5 nm for 10 s evaporation time and 30 ± 5 nm for 15 s. Cross-section SEM of the same samples revealed the expected sponge-like substructure, characteristic for integral asymmetric BCP membranes (Figure 2c,d).<sup>[16,40]</sup>

In the next step, the cross-linking capabilities of the benzophenone moieties were investigated for the pristine statistical copolymer **P1** (without a second block segment). For this purpose, polymer films were fabricated from a THF solution and exposed to 1000 W UV-irradiation for 1–4 min, using a Hönle UV-technology UVA-Cube 2000, equipped with a UVAPRINT 100–200 HPV EZ lamp. For gaining first insights into the cross-linking capabilities of the statistical copolymer, the amount of nonsoluble polymer after irradiation was used to reference the amount of cross-linked polymer material. Interestingly, after 1 min of irradiation 18 wt-% of the polymer was insoluble in THF, increasing to 22 wt-% after 4 min. This result on the amount for cross-linked sites is expected, as mechanistically the benzophenone moieties do not initiate a radical chain reaction and can only form radicals once.<sup>[41]</sup> The upper limit for irradiation time for the BCP membranes was set to 4 min, as the membrane structure collapsed at least after 10 min in previous experiments. Corresponding scanning electron micrographs of differently treated membranes can be found in Figure S3 (Supporting Information). For this purpose, the membranes were subjected to 4 min of UV treatment, carried out in 30 s intervals with 15 s pause in between in order to maximize the content of the cross-linked polymer, while still retaining the porous structure. The pause was applied to allow for heat dissipation upon the irradiation process to prevent destroying the membrane structure. By using this elaborated irradiation protocol, the porous structure of the BCP membrane was obviously retained after the irradiation featuring pore diameters of 29 ± 4 nm for 10 s evaporation time and 30 ± 4 nm for 15 s, which was comparable to the untreated membrane

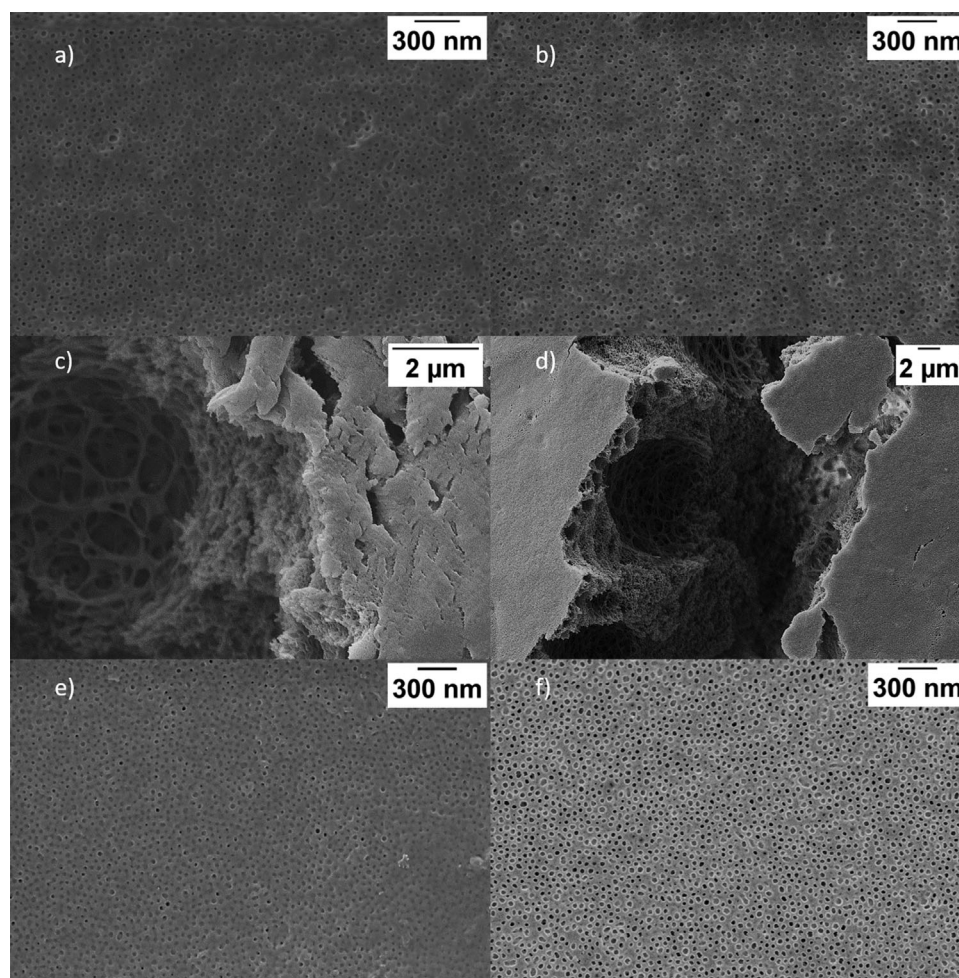


**Figure 2.** Scanning electron micrographs of the P(BMA-*co*-BPMA-*co*-MMA)-*b*-P(HEMA) BCP membranes, fabricated via SNIPS process with different evaporation times and treatments: a) 10 s evaporation time, no treatment b) 15 s evaporation time, no treatment c) 10 s evaporation time, no treatment, inner view of the membrane d) 15 s evaporation time, no treatment, inner view of the membrane e) 10 s evaporation time, 4 min UV-treatment f) 15 s evaporation time, 4 min UV-treatment.

**Table 2.** Summary of the pore diameters, measured from the scanning electron micrographs, shown in Figure 2a,b,e,f). The values presented are the mean of 50 pores.

| Membrane           | 10 s,<br>Untreated | 10 s,<br>UV-treated | 15 s,<br>Untreated | 15 s,<br>UV-treated |
|--------------------|--------------------|---------------------|--------------------|---------------------|
| pore diameter [nm] | 26 ± 5             | 29 ± 4              | 30 ± 5             | 30 ± 4              |

(Figure 2e,f). The pore sizes before and after irradiation, as determined by the mean of 50 pores via SEM imaging, are compiled in Table 2.

To gain additional insights into the swelling behavior and stability of the UV-treated, in comparison to the pristine membrane, the influence of different solvent treatments on the pore size and surface of the BCP membrane was studied by atomic force microscopy<sup>[42]</sup> (AFM; Figure 3; and Figure S4, Supporting Information). For this purpose, the isoporous BCP membrane obtained with 10 s evaporation time before precipitation in water

was used, because this membrane revealed a higher pore order. For the intended measurements, the membranes were stored in the respective solutions for 30 min prior to the AFM measurements to reach the equilibrium state of swelling.

AFM imaging revealed that the distribution of the maximum inscribed radii  $r_m$  of the pores in solution (for both water and ethanol) is shifted to smaller values than those measured in air. The water-ethanol mixture (1:1) led to a further shift to smaller  $r_m$  values compared to pure water, while this trend continued for pure ethanol. This behavior can be explained by the interaction of the different solvents and the polymer block segments. On the one hand, the water was only able to swell the pore forming block, that is the hydrophilic poly(HEMA) block segment, explaining the reduced pore sizes in water. Ethanol on the other hand led to swelling of both the membrane matrix, which is represented by the hydrophobic block segment poly(BMA-*co*-BPMA-*co*-MMA), and the pore forming block poly(HEMA), explaining the further reduction in pore size. After cross-linking reactions of the membrane matrix, this swelling of the hydrophobic block

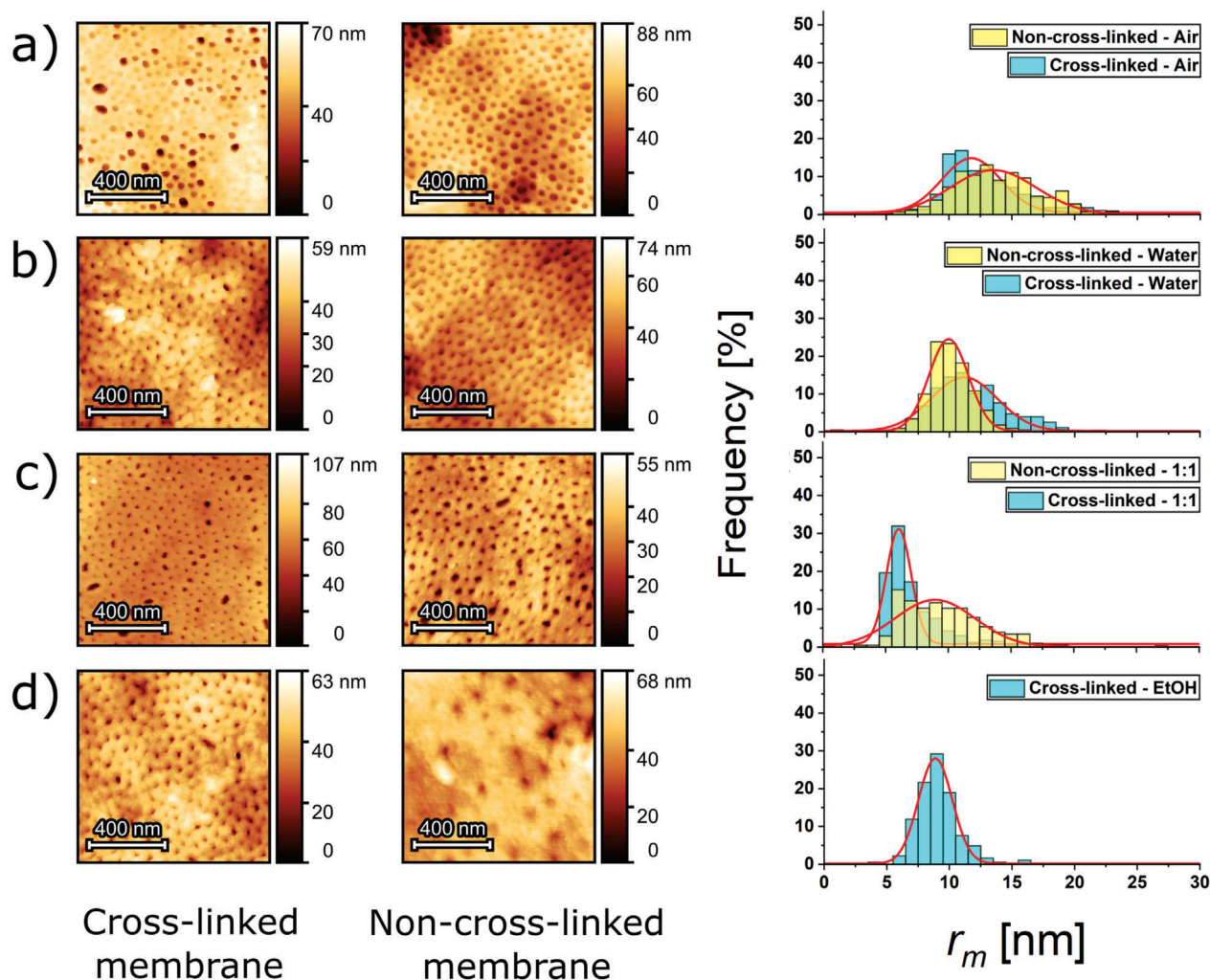


**Figure 3.** Solvent dependency of pore sizes of porous cross-linked and noncross-linked P2 membranes. AFM images and histograms of the maximum inscribed radius  $r_m$  for a) air, b) water, c) water-ethanol (1:1), and d) ethanol. The red lines show Gaussian fits for the data shown in the histograms, respectively.

**Table 3.** Pore sizes of cross-linked and noncross-linked membranes are given for AFM imaging under different environmental conditions. Mean values and error values of the maximum inscribed radius  $r_m$  values are based on the mean values and standard deviations obtained by Gaussian fits given in Figure 3.

| Condition                            | Air        | Water      | Water/Ethanol (1:1) | Ethanol   |
|--------------------------------------|------------|------------|---------------------|-----------|
| $r_{m, \text{cross-linked}}$ [nm]    | $12 \pm 2$ | $11 \pm 3$ | $6 \pm 1$           | $9 \pm 1$ |
| $r_{m, \text{noncross-linked}}$ [nm] | $14 \pm 3$ | $10 \pm 2$ | $9 \pm 3$           | —         |

was significantly reduced in ethanol containing solvent mixtures. Therefore, the cross-linked matrix material was less affected by solvent swelling and the pores stay larger, i.e., similar to values for the water environment (see Table 3). Compared to these findings in presence of ethanol, the pores in pure water did not show a significant change, independent of the presence of cross-linking sites, because the membrane matrix was generally not affected by water.

It can also be concluded from the AFM data that the distributions of the maximum inscribed radii  $r_m$  of the cross-linked sample for the 1:1 water-ethanol mixture are shifted to smaller values than those in pure ethanol (Figure 3c,d). This shift might arise from the fact that the AFM image, for the cross-linked sample exposed to the 1:1 water-ethanol mixture, took 3 h (after 30 min immersion time for equilibration), while the cross-linked membrane sample in pure ethanol could already be obtained within 1 h (after 30 min immersion time for equilibration). This possibly hints toward a time-dependent swelling for the cross-linked membranes, which then overestimates the cross-linked sample for the 1:1 water-ethanol mixture. Nevertheless, a clear decrease in the maximum inscribed radii  $r_m$  of the pores of the noncross-linked membrane structure was observed. The pores collapsed when the noncross-linked membrane was treated with pure ethanol (Figure 3d). The AFM cantilever tip has a finite size that leads to a broadening of the image structures.<sup>[43]</sup> Thus, the indicated maximum inscribed radii  $r_m$  provide a lower limit of the pore radii. As the polymers were not cross-linked here, the

polymer chains had higher mobility in ethanol, and the isoporous structure of the membrane was lost. Accordingly, the characterization of the pore size of the noncross-linked membrane in pure ethanol was not possible. The pore sizes determined for the different conditions are summarized in Table 3. Comparing the pore sizes determined by SEM and AFM imaging, we observed slightly larger pores when using SEM. This difference is accounted for by the measuring method, as with AFM the inscribed radius was measured (see Figure S4, Supporting Information) and in SEM imaging the distance from edge to edge of the pore is measured.

Finally, the behavior of the noncross-linked and cross-linked membrane during the filtration process was compared using the membrane fabricated with 15 s evaporation time. Water flux measurements in a dead-end filtration cell at varying pressures between 0.2 and 0.6 bar were used to investigate the mechanical stability along with the water flux values. The membranes were stored in water for 30 min to reach their equilibrium state of swelling prior to the flux measurement. The cross-linked membrane exhibited a higher water flux for all pressures, with a maximum water flux of  $1358 \text{ L h}^{-1} \text{ bar}^{-1} \text{ m}^{-2}$  for the cross-linked membrane and  $322 \text{ L h}^{-1} \text{ bar}^{-1} \text{ m}^{-2}$  for the untreated membrane at 0.2 bar transmembrane pressure (Table S2, Supporting Information). The higher water flux in the cross-linked state can most likely be explained by a larger pore radius in the swollen state, as evidenced for the membrane with 10 s evaporation time by the AFM images shown in Figure 3. While the absolute values of pore sizes for the 15 s membrane may slightly differ, the relative behavior is expected to remain the same when comparing the cross-linked and noncross-linked membrane.

Furthermore, a higher mechanical stability could be derived from the increased flux at higher transmembrane pressures. Moreover, additional SEM images of the membranes were prepared after the water-flux measurements with varying pressures, proving the pore stability under the applied conditions Figure S5 (Supporting Information).

### 3. Conclusion

In conclusion, a synthetic route to preparing the amphiphilic block copolymer P(BMA-co-BPMA-co-MMA)-b-P(HEMA) was presented featuring a UV-addressable cross-linker moiety based on a benzophenone-containing monomer covalently incorporated within the matrix-forming block segment. After applying the SNIPS process for membrane fabrication, the positive effects of cross-linking the matrix forming block of the block copolymer membrane using UV-irradiation were shown. We confirmed an increased stability against water, ethanol, and mixtures thereof and mechanical pressure using SEM, AFM, and water flux measurements. In the UV-mediated cross-linked membrane, the isoporous top-layer of the membrane was maintained and accompanied by increased swelling resistance. Moreover, there is higher water-flux for all investigated transmembrane pressures compared to the noncross-linked membranes. The herein described approach for direct incorporation of the benzophenone-cross-linker moiety into the block copolymer structure and effect on the stabilization of the membrane will pave the way for a new generation of (isoporous) membranes as selective layer for membrane applications.

### Supporting Information

Supporting Information is available from the Wiley Online Library or from the author.

### Acknowledgements

The authors thank the Deutsche Forschungsgemeinschaft (DFG, German Research Foundation) under Germany's Excellence Strategy – EXC-2193/1 – 390951807 (Q.H. and B.N.B.). This research was partially supported by the DFG Project No. GA2169/7-1 (M.G.) in association with the DFG-funded consortium for advanced paper research (No. DFG-PAK 962/1) at TU Darmstadt. V.P. thanks Eduard Arzt (INM) for his continuing support. Open Access funding enabled and organized by Projekt DEAL.

### Conflict of Interest

The authors declare no conflict of interest.

### Data Availability Statement

Research data are not shared.

### Keywords

amphiphilic polymers, block copolymers, membranes, self-assembly, UV-cross-linking

Received: September 21, 2021

Revised: October 22, 2021

Published online: November 17, 2021

- [1] L. Guo, Y. Wang, M. Steinhart, *Chem. Soc. Rev.* **2021**, 50, 6333.
- [2] S. Kim, K. H. Chu, Y. A. J. Al-Hamadani, C. M. Park, M. Jang, D.-H. Kim, M. Yu, J. Heo, Y. Yoon, *Chem. Eng. J.* **2018**, 335, 896.
- [3] F. Fu, Q. Wang, *J. Environ. Manage.* **2011**, 92, 407.
- [4] L. A. Martin, D. A. L. Vignati, C. Hissler, *Sci. Total Environ.* **2021**, 790, 148207.
- [5] M. Radjabian, V. Abetz, *Progr. Polym. Sci.* **2020**, 102, 101219.
- [6] F. Schacher, M. Ulbricht, A. H. E. Müller, *Adv. Funct. Mater.* **2009**, 19, 1040.
- [7] M. Gallei, S. Rangou, V. Filiz, K. Buhr, S. Bolmer, C. Abetz, V. Abetz, *Macromol. Chem. Phys.* **2013**, 214, 1037.
- [8] S. Schöttner, M. Brodrecht, E. Uhlein, C. Dietz, H. Breitzke, A. A. Tietze, G. Buntkowsky, M. Gallei, *Macromolecules* **2019**, 52, 2631.
- [9] J. I. Clodt, V. Filiz, S. Rangou, K. Buhr, C. Abetz, D. Höche, J. Hahn, A. Jung, V. Abetz, *Adv. Funct. Mater.* **2013**, 23, 731.
- [10] K.-V. P. Suzana Pereira Nunes, *Membrane Technology: in the Chemical Industry*, Wiley-VCH Verlag GmbH & Co. KGaA, Weinheim, Germany **2006**, p. 354.
- [11] J. Vienen, *Membrane Technology*, Vol. 1: Membranes for Life Sciences, Vol. 1 (Eds: K. Peinemann, S. Nunes), Wiley-VCH, Weinheim, Germany **2008**, Ch. 1.
- [12] S. P. Nunes, *Macromolecules* **2016**, 49, 2905.
- [13] L. Upadhyaya, M. Semsarilar, S. Nehache, A. Deratani, D. Quemener, *Eur. Phys. J.: Spec. Top.* **2015**, 224, 1883.
- [14] Y. Zhang, J. L. Sargent, B. W. Boudouris, W. A. Phillip, *J. Appl. Polym. Sci.* **2015**, 132, 41683.
- [15] C. Stegelmeier, A. Exner, S. Hauschild, V. Filiz, J. Perlich, S. V. Roth, V. Abetz, S. Förster, *Macromolecules* **2015**, 48, 1524.

- [16] J. Hahn, J. I. Clodt, C. Abetz, V. Filiz, V. Abetz, *ACS Appl. Mater. Interface* **2015**, 7, 21130.
- [17] K.-V. Peinemann, V. Abetz, P. F. W. Simon, *Nat. Mater.* **2007**, 6, 992.
- [18] C. Regula, E. Carretier, Y. Wyart, G. Gésan-Guizieu, A. Vincent, D. Boudot, P. Moulin, *Water Res.* **2014**, 56, 325.
- [19] C. Höhme, J. Hahn, B. Lademann, A. Meyer, B. Bajer, C. Abetz, V. Filiz, V. Abetz, *Eur. Polym. J.* **2016**, 85, 72.
- [20] J. Zhou, C. Zhang, C. Shen, Y. Wang, *Polymer* **2019**, 164, 126.
- [21] J. K. Elter, J. Eichhorn, F. H. Schacher, *Macromol. Rapid Commun.* **2021**, <https://doi.org/10.1016/j.isci.2020.101204>.
- [22] Y. Chen, A. E. Tavakley, T. M. Mathiason, T. A. Taton, *J. Polym. Sci. Part A: Polym. Chem.* **2006**, 44, 2604.
- [23] T.-H. Kang, H.-I. Lee, *Macromol. Res.* **2019**, 27, 476.
- [24] J. Morsbach, J. Elbert, C. Rüttiger, S. Winzen, H. Frey, M. Gallei, *Macromolecules* **2016**, 49, 3406.
- [25] S. Y. Yang, J. Park, J. Yoon, M. Ree, S. K. Jang, J. K. Kim, *Adv. Funct. Mater.* **2008**, 18, 1371.
- [26] S. Saleem, S. Rangou, C. Abetz, B. Lademann, V. Filiz, V. Abetz, *Polymers* **2017**, 9, 216.
- [27] S. Schöttner, H.-J. Schaffrath, M. Gallei, *Macromolecules* **2016**, 49, 7286.
- [28] S. Schöttner, R. Hossain, C. Rüttiger, M. Gallei, *Polymers* **2017**, 9, 491.
- [29] W. A. Phillip, R. M. Dorin, J. Werner, E. M. V. Hoek, U. Wiesner, M. Elimelech, *Nano Lett.* **2011**, 11, 2892.
- [30] N. D. Carbone, M. Ene, J. R. Lancaster, J. T. Koberstein, *Macromolecules* **2013**, 46, 5434.
- [31] A. Utrata-Wesołek, I. Żymetka-Miara, A. Kowalczyk, B. Trzebicka, A. Dworak, *Photochem. Photobiol.* **2018**, 94, 52.
- [32] C. G. Schäfer, D. A. Smolin, G. P. Hellmann, M. Gallei, *Langmuir* **2013**, 29, 11275.
- [33] C. G. Schäfer, C. Lederle, K. Zentel, B. Stühn, M. Gallei, *Macromol. Rapid Commun.* **2014**, 35, 1852.
- [34] P. Samyn, M. Biesalski, O. Prucker, J. Rühe, *J. Photochem. Photobiol. A: Chem.* **2019**, 377, 80.
- [35] R. Toomey, D. Freidank, J. Rühe, *Macromolecules* **2004**, 37, 882.
- [36] M. Plank, F. Hartmann, B. Kuttich, T. Kraus, M. Gallei, *Eur. Polym. J.* **2020**, 141, 110059.
- [37] S. W. Hughes, *Phys. Educ.* **2005**, 40, 468.
- [38] R. K. Bose, K. K. S. Lau, *Biomacromolecules* **2010**, 11, 2116.
- [39] L. F. Villalobos, M. Karunakaran, K.-V. Peinemann, *Nano Lett.* **2015**, 15, 3166.
- [40] H. Yu, X. Qiu, A. R. Behzad, V. Musteata, D.-M. Smilgies, S. P. Nunes, K.-V. Peinemann, *Chem. Commun.* **2016**, 52, 12064.
- [41] B. Qu, W. Shi, R. Bengt, *J. Photopolym. Sci. Technol.* **1989**, 2, 269.
- [42] Y. F. Dufrêne, T. Ando, R. Garcia, D. Alsteens, D. Martinez-Martin, A. Engel, C. Gerber, D. J. Müller, *Nat. Nanotechnol.* **2017**, 12, 295.
- [43] J. Canet-Ferrer, E. Coronado, A. Forment-Aliaga, E. Pinilla-Cienfuegos, *Nanotechnology* **2014**, 25, 395703.